14TH CANADIAN MASONRY SYMPOSIUM
MONTREAL, CANADA
MAY 16TH – MAY 20TH, 2021

STRUCTURAL MASONRY WALLS WITH RUBBER PADS AND UNBONDED POST-TENSIONING TENDONS: EXPERIMENT AND DESIGN PROCEDURE

Kalliontzis, Dimitrios[1]; Schultz, Arturo E.[2] and Sritharan, Sri[3]

ABSTRACT

The self-centering capability of structural masonry walls can be enhanced with the use of vertical unbonded post-tensioning combined with a rocking mechanism at the wall-foundation interface. However, the lateral displacement capacity of these wall systems is often compromised by early crushing of the compression toes. An experimental research study successfully investigated a new concept to prevent toe crushing by introducing thin rubber pads underneath the bottom corners of a full-scale one-story masonry wall. The wall was subjected to free vibration and quasi-static tests, showing excellent lateral displacement capacity and no observable damage to the masonry. To enable the application of rocking masonry walls with rubber pads and unbonded post-tensioning, this paper presents a design procedure by incorporating different damping components in the response of this wall system, which includes inherent viscous damping, hysteretic action, and energy dissipation due to the wall impacting on the foundation base.

KEYWORDS: *rocking, structural masonry wall, self-centering, rubber pads, seismic*

[1] Assistant Professor, Department of Civil and Environmental Engineering, University of Houston, Houston, TX, United States, dkallion@central.uh.edu
[2] Department Chair and McDermott Professor, Department of Civil and Environmental Engineering, The University of Texas at San Antonio, San Antonio, TX, United States, arturo.schultz@utsa.edu
[3] Interim Associate Dean & Wilkinson Chair Professor, Department of Civil, Construction and Environmental Engineering, Iowa State University, Ames, IA, United States, sri@iastate.edu

INTRODUCTION

As shown in Figure 1a, structural masonry walls with a monolithic connection to the foundation develop their lateral load capacity by means of bonded steel reinforcement. When subjected to lateral loads, these walls can experience significant residual deformations and extensive damage over a region above the wall base. To reduce this damage and improve the self-centering capability of masonry walls, the bonded steel reinforcement can be substituted with unbonded post-tensioned (UPT) tendons, as shown in Figure 1b. Masonry walls with UPT tendons can rock on the foundation base when subjected to lateral loads, which concentrates their inelastic deformations at their bottom corners. Upon removal of the lateral loads, these walls can re-center effectively by means of the restoring tendon forces. In masonry walls with UPT tendons, a minimum amount of embedded steel reinforcement that is terminated within the wall panel may be used for crack control and to prevent shear failure.

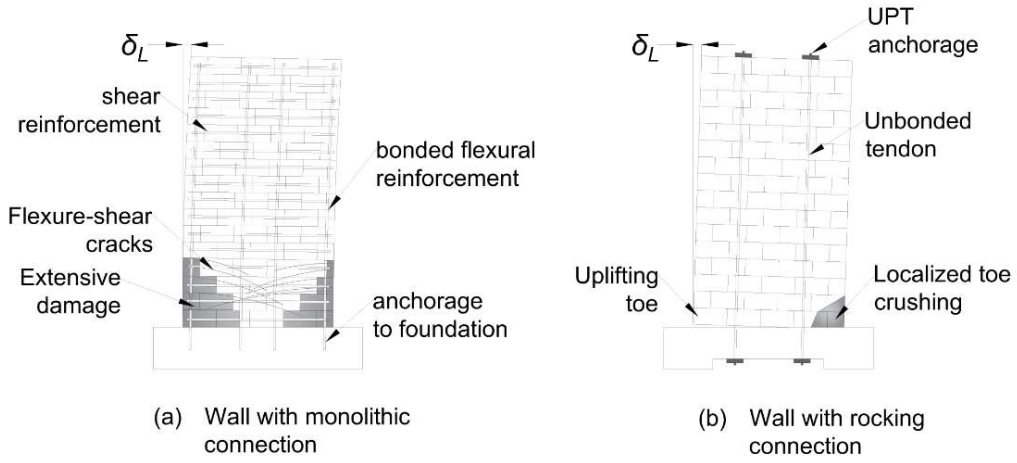

Figure 1: (a) Structural masonry wall with a monolithic connection to the foundation and (b) Structural masonry wall with a rocking connection to the foundation.

The behavior of masonry walls with UPT tendons has been investigated in the past using quasi-static and shake-table tests (e.g., Laursen and Ingham 2001; Rosenboom and Kowalsky 2004; Wight et al. 2006; Hassanli et al. 2016). For the most part, these investigations demonstrated the re-centering capability of masonry walls with UPT tendons and their ability to concentrate damage in the bottom toes (Figure 1b). However, their lateral load behavior may be compromised due to early crushing of the toes, if the toes are not protected.

To prevent toe crushing, Kalliontzis et al. (2021) investigated the use of thin rubber pads underneath the bottom corners of masonry walls with UPT tendons. The goal was to concentrate the majority of nonlinear action in the rubber, minimizing the damage of the masonry toes. Based on the data from this experimental research study, this paper presents a procedure to design the rubber pads and UPT system as well as compute the effective damping in this masonry rocking wall system.

REVIEW OF EXPERIMENTAL RESEARCH STUDY

The experimental research study was conducted in the T. V. Galambos Laboratory at the University of Minnesota to investigate the use of thin rubber pads in a full-scale one-story concrete masonry wall with UPT bars (Kalliontzis et al. 2021). Figure 2 presents the dimensions and reinforcement details of the wall with the thin rubber pads. The wall was fully grouted and constructed using 152-mm concrete masonry units. Its height was 2,438 mm and its length was 1,418 mm. The compressive strength of the masonry was evaluated at 17.6 MPa, using fully grouted masonry prisms. The wall was post-tensioned with two unbonded threaded bars of ASTM A354 Grade BD with a diameter of 15.9 mm. The bars were placed symmetrically in the wall cross-section at a horizontal spacing of 834 mm and within PVC ducts to ensure no bonding with the surrounding grout.

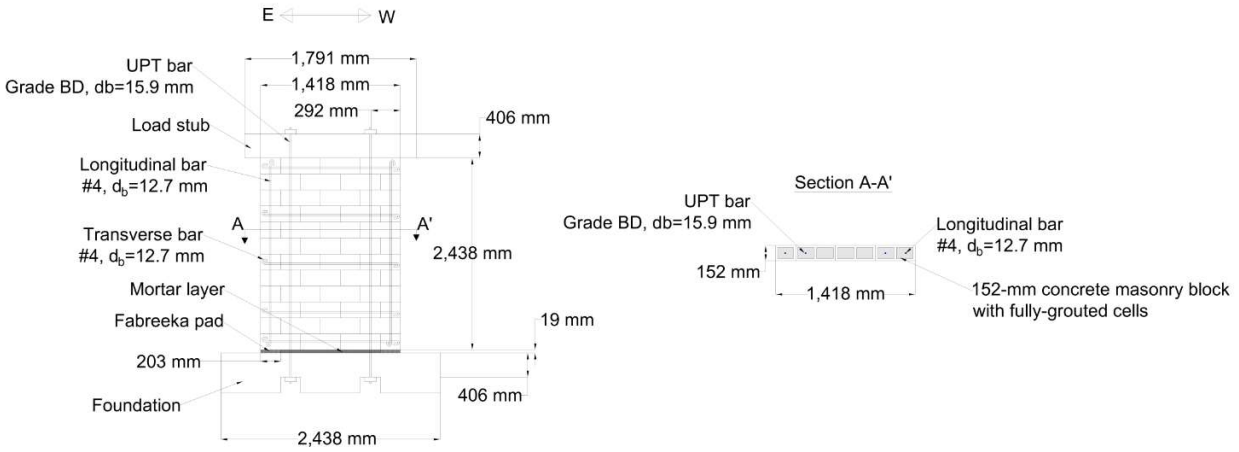

Figure 2: Wall dimensions and reinforcement details.

To protect the wall bottom toes, a resilient reinforced rubber, named as Fabreeka pad (Fabreeka 2015), was used. This rubber pad has a shore hardness of 90 and undergoes small creep deformations when subjected to long-term loads and is resistant to water, mildew, brine, and temperature variations. Using compression tests of three cylindrical specimens in compliance with ASTM D575-18, the compressive strength of the Fabreeka pad was evaluated to be 98.5 MPa at a strain of 0.38 mm/mm, which far exceeded the typical strain demand at the toes of rocking masonry walls (Kalliontzis 2018). Based on the finite element analysis results of the wall by Kalliontzis (2018), the dimensions of the Fabreeka pad were selected to be 203 mm x 19 mm (length x thickness), which were analytically found to adequately reduce the stress concentration in the toe region without compromising the lateral strength of the test wall. Between the Fabreeka pads at the wall toes, a mortar layer with thickness of 19 mm was placed to ensure full contact between the wall and the foundation throughout the wall base length.

The wall was tested using a series of free vibration and quasi-static tests to characterize the energy dissipation capabilities of the wall due to dynamic and hysteretic effects as well as evaluate its lateral load behavior. For the free vibration tests, each unbonded bar was post-tensioned to 245

MPa, resulting in a total initial axial force ratio (A_r) of 2.5%, which included the self-weight of the wall and loading stub. This post-tensioning level was selected to prevent the bars from experiencing nonlinear response, which also helps to isolate the energy dissipation due to dynamic effects as much as possible. Next, the post-tensioning stress was increased to 420 MPa to make the bars respond inelastically at lateral drifts greater than the allowable story drift of 1.0% (ASCE 7-16). More information about the test setup, loading protocols, and instrumentation of the wall can be found in Kalliontzis et al. (2021).

Key test observations

During the free vibration and quasi-static tests, the lateral response of the wall was rocking-dominated with small flexural deformations within the wall panel and negligible horizontal sliding at the wall-foundation interface. Figure 3 presents typical time histories of the total lateral drift and the associated displacement components due to rocking, flexure, and sliding for a test with initial lateral drift at the wall top = 0.75%.

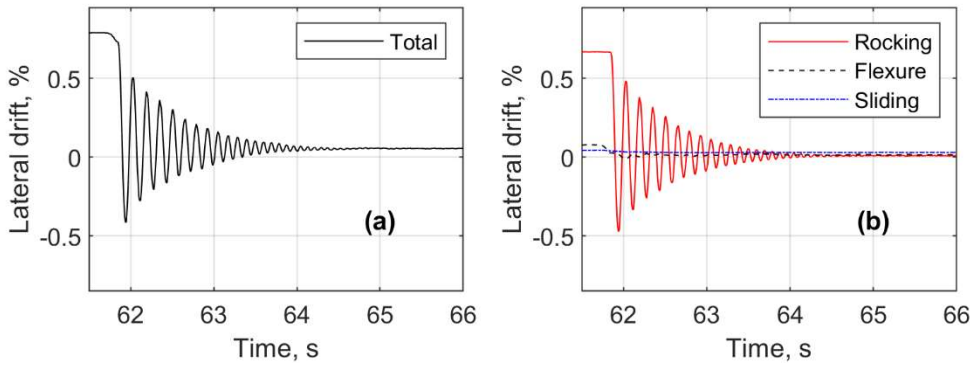

Figure 3: Response of a free vibration test: (a) total lateral drift and (b) displacement components due to rocking, flexure, sliding.

During free vibration tests, the wall underwent impacts with the foundation base, which dissipated part of the wall's kinetic energy. The energy loss was quantified in terms of the coefficient of restitution (r) as follows:

$$r = \left(\frac{\dot{\theta}_2}{\dot{\theta}_1} \right)^2 \tag{1}$$

where $\dot{\theta}_2$ and $\dot{\theta}_1$ = experimental angular velocities of the wall base just before and just after an impact, respectively. The experimentally estimated r was compared with the analytical solution for r of structural rocking members (i.e., Equation 2) proposed by Kalliontzis et al. (2016):

$$r = \left[\frac{1 + \frac{MR_{cm}^{\ 2}}{I_{cm}} \left(1 - \left(sin\alpha\right)^2 \left(1 + k^2\right)\right)}{1 + \frac{MR_{cm}^{\ 2}}{I_{cm}} \left(1 - \left(sin\alpha\right)^2 \left(1 - k^2\right)\right)} \right]^2 \tag{2}$$

where $\alpha = tan^{-1}\left(L_w / \left(2H_{CG}\right)\right)$, with L_w = wall base length and H_{CG} = wall height measured from the foundation base to the center of gravity of the wall and loading stub system; M = total mass of the wall and loading stub; I_{cm} = mass moment of inertia of the wall and loading stub system about its center of gravity; R_{cm} = distance of the same center of gravity from the bottom corner of the wall; and k = 0.72, based on experimental data. Figure 4a compares the test data for r with the analytical solution of Eq. 2. The experimental r values were scattered which was attributed in part to the noise in the collected data near the impact events. However, the test data were fluctuating around the analytical solution, which was equal to 0.81. This was confirmed by calculating the mean value of the test data, which was found to be in excellent agreement with the analytical solution.

Using the logarithmic decrement method, the total damping ratio (ζ_{total}) of the free vibration motions was computed:

$$\zeta_{\text{total}} = ln\frac{d_i}{d_{i+1}} \tag{3}$$

where d_i and d_{i+1} = drifts at two consecutive positive or negative peaks termed $\left(i+1\right)$ and i. The ζ_{total} values were compared with the equivalent viscous damping ratio due to impacts (ζ_{impact}) based on the formula proposed by Kalliontzis and Sritharan (2021):

$$\zeta_{\text{impact}} = -0.15ln\left(r\right) \tag{4}$$

For $r = 0.81$, $\zeta_{\text{impact}} = 3.1\%$. Figure 4b shows that ζ_{total} varied from 3.4% to 5.2%, with the larger damping ratio occurring at drift levels higher than 1.0%. At these drift levels, the average damping ratio from hysteretic and viscous damping effects was 2.0%.

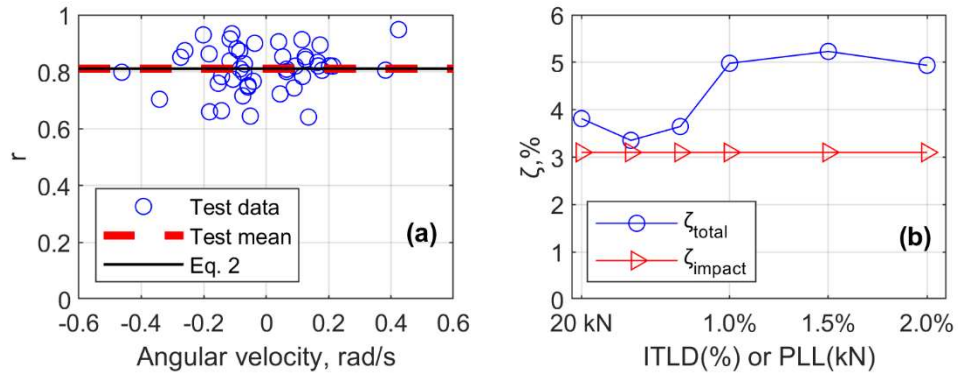

Figure 4: (a) Coefficient of restitution, r and (b) Equivalent viscous damping ratio.

Next, Figure 5 presents the force versus displacement response of the wall during the quasi-static test a) up to the allowable story drift (i.e., ±1.0%); and b) for the entire duration (i.e., up to ± 4.6%). At ±1.0% drifts, the wall resisted loads of 46.2 kN in the positive and 50.3 kN in the negative direction. The maximum lateral load resistance occurred at ±3.9% drifts with 65 kN in the positive and 60 kN in the negative direction. The wall lateral resistance degraded by 8.2% in the positive and 5.2% in the negative direction of loading during the cycles at ±4.6%. Due to reaching the displacement capacity of the actuator, the quasi-static test was terminated at the lateral drift of 4.6%.

Using the Jacobsen's secant stiffness method (Jacobsen 1960), the equivalent viscous damping ratio (ζ_h) due to the hysteretic energy dissipation was computed for the quasi-static test. The values of ζ_h varied from 2.6% at lateral drifts below 1.0% to 6.4% at the last cycles of the test for the drift of 4.6%. For lateral drifts up to 2.0%, the average ζ_h was computed to be 3.3%. Of this value, 0.7% was attributed to the horizontal sliding of the wall with respect to the foundation base and 2.6% was estimated to be due to the hysteretic action of the Fabreeka pads and UPT bars. Additional information on the experimental data analysis can be found in Kalliontzis et al. (2021).

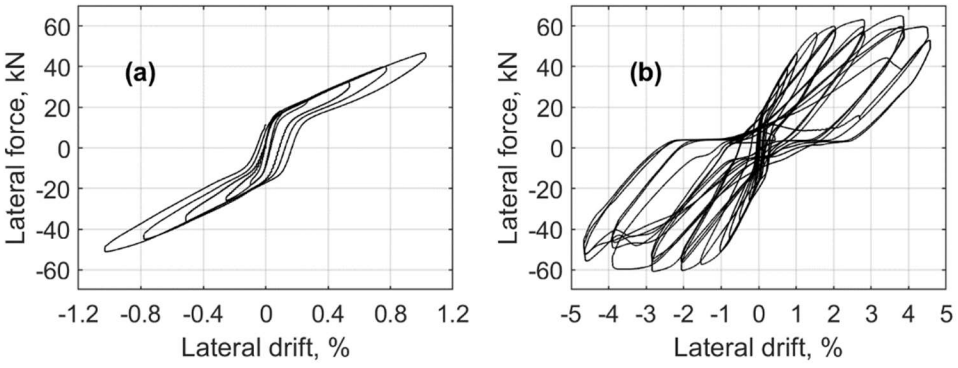

Figure 5: Lateral force versus lateral displacement response of the wall (a) up to 1.0% lateral drift and (b) the complete test.

DESIGN PROCEDURE

Following the experimental study, a procedure is developed to enable appropriate selection of thin rubber pads and bars in the design of one-story masonry walls with unbonded post-tensioning. The proposed procedure is based on the following assumptions:

1. The maximum lateral drift ratio for the wall is 2.0%
2. Horizontal sliding at the wall-foundation interface and flexure within the wall panel are neglected, assuming that rocking dominates the lateral load behavior of the wall.
3. The wall is rectangular with a height-to-width ratio greater than 2.0. The wall is fully grouted and reinforced per TMS 402-16 with all bonded reinforcement terminating within the wall panel; i.e., not extended into the foundation.
4. Wall dimensions and material properties of the masonry, UPT bars, and rubber are known.
5. The wall is used in low-rise building construction (ASCE 7-16).
6. The foundation of the wall is designed as a capacity-protected member.

Design of Rubber Pads and UPT bars

Fabreeka-like rubber pads can be used. For structural rocking walls, the thickness of the pads can vary from 12.7 mm to 25.4 mm (Kalliontzis and Sritharan 2021). The UPT system can include one or multiple bars. The wall self-weight and the initial post-tensioning force should result in a total initial axial force ratio (A_r) between 2% and 10%. The lower bound of 2% is used to ensure that horizontal sliding of the wall on the foundation base is prevented by adequate lateral frictional resistance. The upper bound of 10% is used to avoid large stress concentrations at the compression wall toes. The following steps are proposed for the design of the rubber pads and the UPT bars:

Step 1: Select A_r

Using A_r, the total initial post-tensioning force ($P_{t,i}$) is calculated:

$$P_{t,i} = -P_w + A_r \left(A_g f'_m \right) \tag{5}$$

where P_w = compressive axial load due to self-weight; A_g = gross cross-sectional area of the masonry wall; and f'_m = compressive strength of masonry.

Step 2: Select number of UPT bars (N_b)

The number of UPT bars should be selected to ensure that there is no bar within the compression region of the wall toes. The length of this region at the wall base is taken as the contact length at the allowable 1.0% lateral drift, which is calculated in Step 5. Next, the initial post-tensioning force per bar is computed as $P_{b,i} = P_{t,i} / N_b$.

Step 3: Select bar sizes

The selection of bar sizes is based on the lateral load demand imposed on the wall. Additionally, it needs to ensure that the initial post-tensioning stresses are sufficiently below the proportional stress limit of the bars to avoid premature inelastic action. A lower bound for the bar sizes is used

to ensure adequate lateral frictional resistance at the wall-foundation interface. The initial post-tensioning stress is suggested to be between 20% and 80% of the proportional stress limit:

$$\frac{P_{b,i}}{0.2 f_{pl}} \geq A_b \geq \frac{P_{b,i}}{0.8 f_{pl}} \tag{6}$$

where A_b = cross-sectional area of one UPT bar; and f_{pl} = proportional stress limit of the bar.

Step 4: Select thickness of the rubber pads (Z_R)

The rubber pad thickness (Z_R) can be selected such that 12.7 mm $\leq Z_R \leq$ 25.4 mm. If a wall taller than one story is designed, this range can be revised with additional test and/or computational data.

Step 5: Estimate contact length ($c_{1\%}$) at 1.0% lateral drift and rubber pad length (L_R)

The wall-foundation contact at the lateral drift of 1.0% is termed $c_{1\%}$. It is obtained by satisfying vertical equilibrium between the compressive forces of the rubber, the self-weight of the wall and loading stub, and the UPT bar forces. The vertical equilibrium condition is satisfied using an iterative procedure as shown in Figure 6, from which the value of $c_{1\%}$ is calculated.

In the iterative procedure, the stress in the UPT bars and rubber pads can be obtained using the Menegotto and Pinto (1973) model (M-P model):

$$\sigma^*\left(\varepsilon^*\right) = b\varepsilon^* + \frac{\left(1-b\right)\varepsilon^*}{\left(1+\left(\varepsilon^*\right)^R\right)^{1/R}} \tag{7}$$

with $\varepsilon^* = \varepsilon / \varepsilon_0$ and $\sigma^* = \sigma / \sigma_0$, where ε_0 and σ_0 = strain and stress values at the meeting point of the two asymptotes of the M-P model, respectively. The values of ε_0 and σ_0 are calibrated for the UPT bars and the rubber pads as shown in the next section. Moreover, R is a dimensionless parameter that is also calibrated for each material, and

$$b = E_1 / E_0 \tag{8}$$

where E_0 = slope of the first asymptote. For UPT bars, E_0 represents the modulus of elasticity of the bars and, for rubber pads, it represents the initial tangent modulus of the rubber. E_1 = slope of the second asymptote, which represents the tangent modulus at the ultimate strength of each material. Experimentally calibrated values of ε_0, σ_0, R, E_0, and E_1 for UPT bars and rubber pads are presented in the next section. Additionally, ε and σ = current strain and stress values, respectively. The tensile strain in the j^{th} UPT bar ($\varepsilon_{b,j}$) is equal to the effective strain due to the

initial post-tensioning force plus the uplift displacement of the wall base at the bar location over the unbonded length of the bar (L_u):

$$\varepsilon_{b,j}\left(x_{b,j}\right)=\varepsilon_{b,0}+\frac{0.01\left(x_{b,j}-c_{1\%}\right)}{L_u} \tag{9}$$

where $\varepsilon_{b,0}$ = effective strain due to the initial post-tensioning force; $x_{b,j}$ = distance of the UPT bar from the extreme compression fiber of the wall base. The total force by the UPT bars (P_{PT}) is computed as:

$$P_{PT}=\sum_{j=1}^{N_b}\sigma_{b,j}\left[\varepsilon_{b,j}\left(x_{b,j}\right)\right]A_{b,j} \tag{10}$$

where $\sigma_{b,j}$ = tensile stress in the j^{th} bar. The compressive strain in a rubber fiber (ε_R) is estimated as the compression of the wall base at the fiber location over an equivalent compression height. This height is estimated as the addition of the pad thickness (Z_R) and a height Z_c , which is the compression zone in the masonry wall above the pads (Kalliontzis and Schultz 2017). An estimate of $Z_c=0.3\%H_w$ is used, where H_w = masonry wall height. Then, ε_R becomes:

$$\varepsilon_R\left(x_R\right)=\frac{0.01\left(c_{1\%}-x_R\right)}{\left(Z_c+Z_R\right)} \tag{11}$$

The total compressive rubber force (P_R) is computed as follows:

$$P_R=t_w\int_0^{L_R}\sigma_R\left[\varepsilon_R\left(x_R\right)\right]dx_R \tag{12}$$

where t_w = wall thickness; σ_R = compressive stress in the rubber fiber; x_R = distance of the fiber from the extreme compression fiber; and L_R = length of the rubber pad, which is taken as $L_R=2c_{1\%}/3$ based on the experimental data in Kalliontzis et al. (2021).

Step 6: Check UPT bar stresses at 1.0% lateral drift

Check the UPT bar stresses from **Step 5** to ensure that the extreme bar near the uplifting toe reaches the proportional stress limit at the drift of 1.0%. If this condition is not satisfied within an acceptable tolerance, revisit the design of the UPT system in **Steps 1-3**. Otherwise, proceed to **Step 7**.

Step 7: Estimate lateral load resistance of the wall

The moment resistance at the wall base for the allowable story drift of 1.0% and the drift of 2.0% are calculated as:

$$M_r = P_w R_{cm} sin\left(\alpha - \theta_b\right) + \sum_{i=1}^{N_b} \sigma_{b,i}\left[\varepsilon_{b,i}\left(x_{b,i}\right)\right] A_b x_{b,i} + t_w \int_0^{L_R} \sigma_R\left[\varepsilon_R\left(x_R\right)\right] x_R dx_R \tag{13}$$

where R_{cm} and α are the same as in Equation 2; and θ_b = 0.01 or θ_b = 0.02. Assuming a planar horizontal load at H_L, the lateral load resistance of the wall becomes:

$$F_r = M_r / H_L \tag{14}$$

If F_r is not adequate, go back to **Steps 1-3**. Revising the wall dimensions may also be examined.

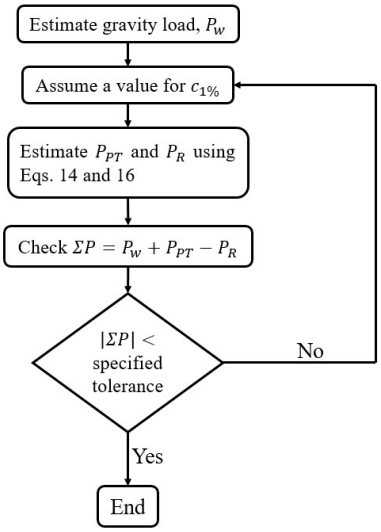

Figure 6: Iterative procedure for calculating $c_{1\%}$.

Equivalent viscous damping ratio

The effective damping of the wall (ζ_{eff}) is computed as:

$$\zeta_{eff} = \zeta_{\text{impact}} + \zeta_{\text{h}} \tag{15}$$

where ζ_{impact} is estimated with Equations 2 and 4. The value of ζ_{h} is taken to be 2.6%, with consideration to the hysteretic damping from the rubber pads and the UPT bars.

EXAMPLE

The design procedure is demonstrated for the wall specimen of Figure 2.

Step 1: Select a value of $A_r = 0.04$, which satisfies $0.02 \leq A_r \leq 0.10$. The compressive axial load due to self-weight of the wall and loading stub is $P_w = 20.1$ kN. Using Equation 5, $P_{t,i} = 122.5$ kN.

Step 2: Two unbonded bars, $N_b = 2$, are spaced as shown in Figure 2 with $P_{b,i} = 122.5/2 = 61.25$ kN.

Step 3: Select ASTM A354 Grade BD bars with $A_b = 146$ mm^2; i.e., $101 \leq A_b \leq 403$, which satisfies Equation 6.

Step 4: Select $Z_R = 19$ mm, which satisfies $12.7 \text{ mm} \leq Z_R \leq 25.4$ mm.

Step 5: Use the iterative procedure of Figure 6 with the modeling parameters of Table 1. A contact length of $c_{1\%} = 301$ mm is estimated with an acceptable error of 0.02 kN. This leads to $L_R = \frac{2c_{1\%}}{3} = 200$ mm, which agrees well with the experimental values in Kalliontzis et al. (2021). Select $L_R = 203$ mm, which corresponds to a half-length concrete masonry unit used in the wall of Figure 2.

Step 6: A value of $\sigma_b = 758$ MPa is calculated for the stress in the unbonded bar near the uplifting toe of the wall. This estimate agrees well with the proportional limit of 760 MPa.

Step 7: Using Equations 13 and 14, $F_r = 53$ kN for the 1.0% drift and $F_r = 61$ kN for the 2.0% drift, which compare adequately with the experimental values of 46.2/50.3 kN (i.e., positive/negative direction) and 60.2/59.7 kN, respectively.

Equivalent viscous damping ratio

From Equation 15, $\zeta_{eff} = \zeta_{\text{impact}} + \zeta_{\text{h}} = 3.1\% + 2.6\% = 5.7\%$.

Table 1: Modeling parameter selection for the M-P models of UPT bars and rubber pad.

Parameter	Material	
	UPT bar	Rubber pad
ε_0	0.01	0.30
σ_0	1.1 f_{pl}	55 MPa
E_0	190,000 MPa	80 MPa
E_1	0.025 E_0	6.5 E_0
R	6.0	3.0

CONCLUSIONS

Structural masonry walls designed with unbonded post-tensioning (UPT) may experience early crushing of their bottom toes due to the large compressive forces imposed on them. To prevent toe crushing, an experimental study investigated the use of thin rubber pads at the toe regions of these walls. Based on the experimental results of this study, the present paper developed a design procedure for the use of thin rubber pads in masonry walls with unbonded post-tensioning. The procedure accounts for the selection of the rubber pads and design of the UPT bars assuming a design lateral drift level of 1.0% (ASCE 7-16) and a maximum lateral drift of 2.0%. The procedure estimates the effective damping ratio provided by this wall system, accounting for the hysteretic action of the rubber pads and UPT bars as well as the impact damping of the wall due to rocking motion. The procedure was shown to estimate the lateral strength and damping of this masonry wall system with good accuracy.

REFERENCES

[1] Laursen, P. T. and Ingham J. M. (2001). "Structural testing of single-storey post-tensioned concrete masonry walls." *TMS Journal*, 69-82.

[2] Rosenboom O. A. and Kowalsky M. J. (2004). "Reversed in-plane cyclic behavior of post-tensioned clay brick masonry walls." *ASCE Journal of Structural Engineering*, 130(5), 787-798.

[3] Wight G. D., Ingham J. M. and Kowalsky M. J. (2006). "Shaketable testing of rectangular post-tensioned concrete masonry walls." *ACI Structural Journal*, July-August, 587-595.

[4] Hassanli R., ElGawady A. and Mills J. E. (2016). "Experimental investigation of in-plane cyclic response of unbonded posttensioned masonry walls." ASCE Journal of Structural Engineering, 142(5), May 2016. https://doi.org/10.1061/(ASCE)ST.1943-541X.0001450.

[5] Kalliontzis D., Schultz A. E., and Sritharan S. (2021). "Unbonded post-tensioned structural masonry wall with rubber interface for limited-damage systems." *ASCE Journal of Structural Engineering* (under review).

[6] ASTM (American Society for Testing and Materials). 2018. "Standard specification for quenched and tempered alloy steel bolts, studs, and other externally threaded fasteners." ASTM A354, West Conshohocken, PA: ASTM.

[7] Fabreeka. 2015. "Vibration and shock control: Reducing structure-borne noise & impact shock and vibration." *Technical Report*, Fabreeka International, Inc., Stoughton, MA.

[8] ASTM (American Society for Testing and Materials). 2018. "Standard test methods for rubber properties in compression." ASTM D575-18, West Conshohocken, PA: ASTM.

[9] Kalliontzis D. (2018). "Behavior of precast concrete and masonry wall systems with jointed connections subjected to lateral loads." PhD dissertation, Department of Civil, Environmental, and Geo- Engineering, University of Minnesota, Twin Cities, Minnesota, United States.

[10] ASCE (American Society of Civil Engineers). *Minimum design loads and associated criteria for buildings and other structures*. 2016. ASCE/SEI 7-16. Reston, Virginia: ASCE.

[11] Kalliontzis D., Sritharan S. and Schultz A. E. (2016). "Improved coefficient of restitution estimation for free rocking members." *ASCE Journal of Structural Engineering*, 142(12), December 2016, https://doi.org/10.1061/(ASCE)ST.1943-541X.0001598.

[12] Kalliontzis D. and Sritharan S. (2021). “Seismic behavior of unbonded post-tensioned precast concrete members with thin rubber layers at the jointed connection.” *PCI Journal*, 66(1), 60-76.
[13] Jacobsen L. S. (1960). “Damping in composite structures.” *Proceedings of the 2nd World Conference on Earthquake Engineering*, 1029-1044, 2, Tokyo and Kyoto, Japan.
[14] Menegotto M. and Pinto P. E. (1973). “Method of analysis of cyclically loaded RC plane frames including changes in geometry and non-elastic behavior of elements under normal force and bending.” *Preliminary Report IASBE*, vol. 13.
[15] Kalliontzis D. and Schultz A. E. (2017). ‘Improved estimation of the reverse-cyclic behavior of fully grouted masonry shear walls with unbonded post-tensioning.” *Engineering Structures*, 145, 83-96.